48. Matsumoto, T., Tokonami, M. & Morimoto, N. *Am. Miner.* **60**, 634–641 (1975).
49. Bruno, E., Carbonin, S. & Molin, G. *Tschermaks Miner. Petrogr.* **29**, 223–240 (1982).
50. Pannhorst, W., *Neues Jb. Miner. Abh.* **150**, 209–218 (1984).
51. Rayner, J. H. & Brown, G. *Clays Clay Minerals* **21**, 103–114 (1973).
52. Lee, J. H. & Guggenheim, S. *Am. Miner.* **66**, 350–357 (1981).
53. Prince, E. *Am. Miner.* **56**, 1243–1251 (1971).
54. Drits, V. A. & Kashaev, A. A. *Kristallografiya* **5**, 224–227 (1960).
55. Phillips, M. W., Gibbs, G. V. & Ribbe, P. H. *Am. Miner.* **59**, 79–84 (1974).
56. Guggenheim, S. *Am. Miner.* **66**, 1221–1232 (1981).
57. Shirozu, H. & Bailey, S. W. *Am. Miner.* **51**, 1124–1143 (1966).
58. Rayner, J. H. *Miner. Mag.* **39**, 850–856 (1974).
59. Gueven, N. & Burnham, C. W. *Carnegie Inst. Wash. Yb.* **65**, 290–293 (1966).
60. Iakeuchi, Y. *Clays Clay Minerals* **13**, 1–25 (1966).
61. Tagai, T., Ried, H., Joswig, W. & Korekawa, M. *Z. Kristallogr.* **160**, 159–170 (1982).
62. Dollase, W. A. *Z. Kristallogr.* **121**, 369–377 (1965).
63. Le Page, Y. & Donnay, G. *Acta crystallogr.* **32**, 2456–2459 (1976).
64. Levien, L. & Papike, J. J. *Am. Miner.* **61**, 864–877 (1976).
65. Harlow, G. E. & Brown, G. E. B. Jr *Am. Miner.* **65**, 986–995 (1980).
66. Ferguson, R. B. & Traill, R. J. *Acta crystallogr.* **25**, 1503–1517 (1969).
67. Morosin, B. *Acta crystallogr.* **28**, 1899–1903 (1972).
68. Hawth[illegible]me, F. C. & Cerny, P. *Can. Miner.* **15**, 414–421 (1977).
69. [illegible], B. E. & Bailey, Y. W. *Acta crystallogr.* **17**, 1391–1400 (1964).

Thermodynamic stability of a smectic phase in a system of hard rods

D. Frenkel*, H. N. W. Lekkerkerker† & A. Stroobants†

* FOM Institute for Atomic and Molecular Physics, PO Box 41883, 1009 DB Amsterdam, The Netherlands
† Van 't Hoff Laboratory, University of Utrecht, Padualaan 8, 3584 CH Utrecht, The Netherlands

One of the most remarkable phenomena exhibited by colloidal suspensions of monodisperse rod-like particles is the spontaneous formation of smectic liquid crystals[1–5]. In these smectic phases, the particles order in periodic layers; on average, the axes of the rods are perpendicular to the layers. Smectics are distinct from crystals in that there is no long-range positional order within the layers. Because the spacing of the smectic layers is of the order of optical wavelengths, white light is separated into colours when scattered, giving rise to beautiful iridescence as in the colour photographs of ref. 2. As early as 1949, Onsager[6] showed that nematic ordering may arise from hard-core repulsions between anisometric particles. However, it appears to have been generally accepted in the literature that smectic liquid crystalline ordering demands that attractive forces also operate[7]. There is nevertheless experimental evidence that smectic ordering does occur in colloidal systems where the particles interact predominantly through repulsive electrostatic interactions. This observation raises the fundamental question of whether smectic ordering can occur in a system of particles with purely repulsive interactions. Inspired by the seminal work of Alder and Wainwright[8] on the freezing of a system of hard spheres, we have explored the possibility that smectic ordering occurs in a fluid of hard rod-like particles. Earlier computer simulations on hard parallel spherocylinders[9,10] (cylinders with length L and diameter D, capped at each end with hemispheres of the same diameter) indicated that, in this somewhat artificial system, smectic order was indeed possible. Here we present numerical evidence that hard spherocylinders with both translational and orientational freedom can form a thermodynamically stable smectic phase.

Molecular dynamic calculations (MD) and constant pressure Monte Carlo simulations (MC) were done on a system of 576 hard spherocylinders with $L/D=5$. Periodic boundary conditions were imposed to minimize the effect of finite system size. Initially the spherocylinders were arranged in a face-centred cubic crystal which was expanded along the [111] axis by a factor $1+L/D$. The shape of the resulting simulation box was very nearly cubic. This close-packed lattice was then expanded to five times its original volume. At this low density the spherocylinders form a translationally and orientationally disordered fluid. Visual inspection of snapshots of the arrangements of the particles and computation of the appropriate order parameters confirmed that the fluid at 20% of close packing was free of residual positional and orientational order. The fluid was slowly compressed to higher densities. Typically, the density was increased in steps of 5% of the close-packed density. At every new density the system was equilibrated for at least 10,000 trial moves per particle (cycles), followed by alternating MC and MD production runs. The typical length of the MD runs was $1\text{–}2\times10^6$ collisions and the MC runs consisted of 20,000 cycles. Close to phase transitions it was generally necessary to equilibrate for much longer. Figure 1 shows the equation-of-state data obtained in these simulations.

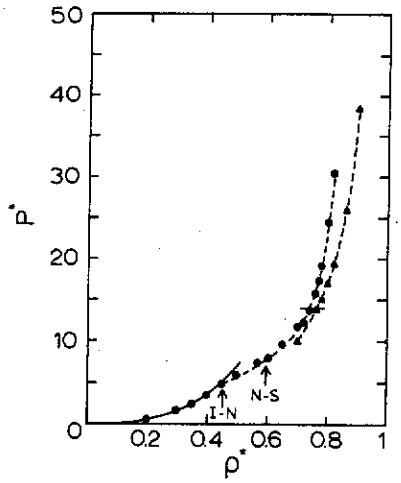

Fig. 1 Equation of state of hard spherocylinders with $L/D=5$. The reduced density ρ^* equals ρ/ρ_{cp}, where ρ_{cp} is the density at regular close packing. The reduced pressure P^* is defined as Pv_0/kT, where v_0 is the volume per particle. The circles denote the molecular dynamics results for the pressure in the fluid phase, and the triangles correspond to the crystalline branch. The dashed curves are numerical fits to the data points. The drawn curve represents a five-term virial series, evaluated using the virial coefficients of this model system, which had been computed separately[12]. The location of the isotropic–nematic and nematic–smectic phase transitions (see text) are indicated by arrows. The horizontal bar at $P^*=13.8$ connects the densities of the coexisting smectic and crystalline phases.

At a density corresponding to 45% of regular close packing, the system was observed to transform spontaneously into an orientationally ordered fluid. Analysis of the long-range orientational and positional correlations in this phase indicated that it was in fact a nematic liquid crystal.

Upon further compression an increase was noted in the amplitude of a particular Fourier component of the density fluctuations, namely the one with a wave-vector of order $2\pi/(L+D)$ pointing along the nematic director. As the density increased, the amplitude of this Fourier component grew, as did its decay time. At 60% of close packing, the system developed a static one-dimensional density modulation along the director, but no translational ordering was observed in the directions perpendicular to the director. Such one-dimensional ordering is the hallmark of a smectic-A liquid-crystalline phase. A typical example of the instantaneous arrangement of the particles in this phase is shown in Fig. 2. Although the fact that the latter phase formed spontaneously on compression indicates that it is stable with respect to both the isotropic and the nematic phases, its thermodynamic stability with respect to the crystalline state remained to be established. To this end we computed the

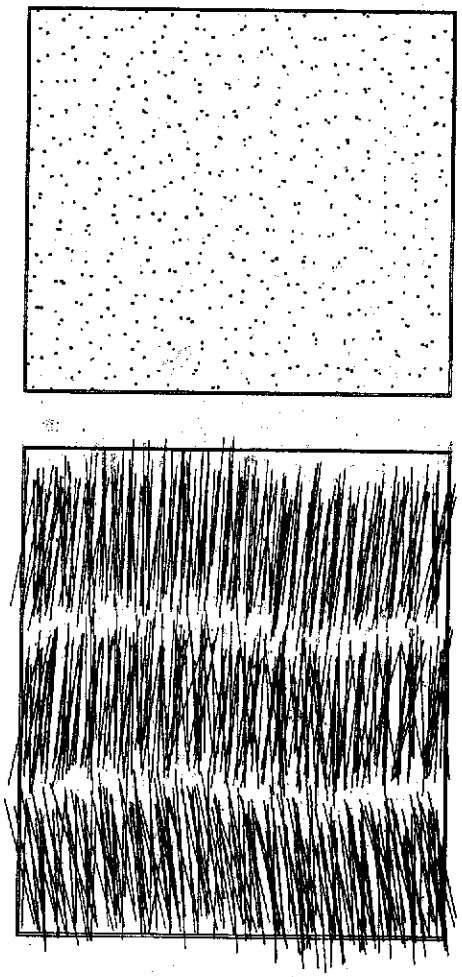

Fig. 2 Typical example of a configuration of 576 hard spherocylinders in the smectic-A phase ($\rho^* = 0.65$). The lower figure shows a side view of the orientationally ordered fluid. For clarity, the spherocylinders are represented by line segments of length L. The upper figure shows a projection of the centres of mass of the particles (dots) on a plane perpendicular to the direction of orientational alignment. Note that there is no translational order in this plane.

chemical potential of the solid phase at a reduced density of 0.86 using the techniques described in ref. 11. The equation-of-state of the crystalline solid was obtained by (constant-stress) MC and MD simulation on systems of 144 spherocylinders with density between 70% and 90% of close packing. The chemical potential of the fluid phase was obtained by thermodynamic integration from the dilute gas. This integration of the fluid equation-of-state was achieved by fitting the numerical equation-of-state data to a polynomial in $\phi/(1-\phi)$, where ϕ is the volume fraction. The polynomial was integrated analytically. The fluid-solid coexistence point was then found by locating the densities at which the pressure and chemical potential of the two phases were equal. Using this procedure we found that a smectic phase with a density of 73% of close packing coexists with a crystalline solid with a density of 76% of close packing.

The nematic to smectic transition is accompanied by pre-transitional fluctuations usually associated with a continuous phase transition, but the system size used did not allow us to distinguish unambiguously between a continuous phase transition and a weakly first-order one. The phase transition from the smectic phase to the crystalline solid is first order. The jump in the density at this transition is ~4%, and should be compared with a value of ~10% for the corresponding quantity at the fluid-solid transition in a hard sphere system. Finally, it is amusing to note that in the system studied here the width of the range of stability of the 'unexpected' smectic phase is comparable with that of the nematic phase.

This work is part of the research programme of Foundation for Fundamental Research of Matter (FOM) with financial support from Netherlands Organisation for Pure Research (ZWO).

Received 20 November 1987; accepted 27 January 1988.

1. Oster, G. *J. gen. Physiol.* **33**, 445–473 (1950).
2. Kreibig, U. & Wetter, C. *Z. Naturforsch.* **35C**, 750–762 (1980).
3. Fraden, S., Hurd, A. J., Meyer, R. B., Cahoon, M. & Caspar, D. L. D. *J. Phys.* (Paris), *Colloq.* **46** C3, 85–113 (1985).
4. Maeda, Y. & Hachisu, S. *Colloids and Interfaces* **6**, 1–16 (1983).
5. Maeda, Y. & Hachisu, S. *Colloids and Interfaces* **7**, 357–360 (1984).
6. Onsager, L. *Ann. N.Y. Acad. Sci.* **51**, 627–659 (1949).
7. Kloczkowski, A. & Stecki, J. *Molec. Phys.* **55**, 689–700 (1985).
8. Alder, B. J. & Wainwright, T. E. *J. Chem. Phys.* **27**, 1208–1209 (1957).
9. Stroobants, A. Lekkerkerker, H. N. W. & Frenkel, D. *Phys. Rev. Lett.* **57**, 1452–1455 (1986).
10. Stroobants, A., Lekkerkerker, H. N. W. & Frenkel, D. *Phys. Rev.* **A36**, 2929–2945 (1987).
11. Frenkel, D. & Mulder, B. M. *Molec. Phys.* **55**, 1171–1192 (1985).
12. Frenkel, D. *J. phys. Chem.* (in the press).

Majorite fractionation recorded in the geochemistry of peridotites from South Africa

Claude Herzberg*, Mark Feigenson*, Cherylyn Skuba† & Eiji Ohtani‡

* Department of Geological Sciences, Rutgers University, New Brunswick, New Jersey 08903, USA
† Department of Geology, University of Texas at Arlington, Arlington, Texas 76019, USA
‡ Department of Earth Sciences, Ehime University, Matsuyama 790, Japan

The liquidus phase for ultrabasic rock compositions changes from olivine at low pressures to a pyroxene polymorph at high pressures[1,2]. In the range 13–25 GPa, the liquidus phase for a chondritic bulk Earth composition is majorite[3,4], a pyroxene with the garnet crystal structure. For upper-mantle lherzolite compositions, majorite is also the liquidus phase from ~16–25 GPa[5–7], and transforms to perovskite at similar or higher pressures[7]. As majorite has a density higher than peridotite magmas[8,9], it could have fractionated during an early differentiation event in the Earth[3]. Here we argue that this process is recorded in the major-element geochemistry of peridotites from South Africa, and that it has resulted in a lower mantle enriched in silica.

Figure 1*a* shows in projection the major-element geochemistry of a world database for peridotites. The compilation of Maaloe and Aoki[10] has been used ($N = 504$), and upgraded in this study to include more recent analyses ($N = 1{,}040$). There is a clear bifurcation in this plot, with most peridotites from South Africa occupying the right-hand trend and most peridotites from the rest of the world occupying the left-hand trend. For the purpose of clarification, the two populations of data are plotted separately in Fig. 1*b* (world database excluding samples from South Africa) and Fig. 1*c* (samples from South Africa). The South African samples from the continental lithosphere consist largely of the orthopyroxene-rich granular garnet lherzolite and garnet harzburgite xenoliths. The fertile sheared garnet lherzolites from South Africa, which are not as abundant and are thought to be pieces of asthenosphere[11], are plotted in the left-hand trend defined mainly by spinel peridotites from the rest of the world. Harzburgite residua from ophiolite complexes occupy the point of the V in Fig. 1*a*.

Superimposed on the geochemistry of mantle peridotite are the locations of the experimentally constrained primary phase